JACS
JOURNAL OF THE AMERICAN CHEMICAL SOCIETY

Article

pubs.acs.org/JACS

Amplifying Dynamic Nuclear Polarization of Frozen Solutions by Incorporating Dielectric Particles

Dominik J. Kubicki,[†] Aaron J. Rossini,[†] Armin Purea,[‡] Alexandre Zagdoun,[†] Olivier Ouari,[§] Paul Tordo,[§] Frank Engelke,[‡] Anne Lesage,[†] and Lyndon Emsley*[,†,∥]

[†]Institut de Sciences Analytiques (CNRS/ENS de Lyon/UCB-Lyon 1), Centre de RMN à Très Hauts Champs, Université de Lyon, 69100 Villeurbanne, France

[‡]Bruker Biospin GmbH, Silberstreifen, D-76287 Rheinstetten, Germany

[§]Aix Marseille-Université, CNRS, ICR UMR 7273, 13397 Marseille, France

[∥]Institut des Sciences et Ingénierie Chimiques, Ecole Polytechnique Fédérale de Lausanne (EPFL), CH-1015 Lausanne, Switzerland

Supporting Information

ABSTRACT: There is currently great interest in understanding the limits on NMR signal enhancements provided by dynamic nuclear polarization (DNP), and in particular if the theoretical maximum enhancements can be achieved. We show that over a 2-fold improvement in cross-effect DNP enhancements can be achieved in MAS experiments on frozen solutions by simply incorporating solid particles into the sample. At 9.4 T and ∼105 K, enhancements up to ε_H = 515 are obtained in this way, corresponding to 78% of the theoretical maximum. We also underline that degassing of the sample is important to achieve highest enhancements. We link the amplification effect to the dielectric properties of the solid material, which probably gives rise to scattering, diffraction, and amplification of the microwave field in the sample. This is substantiated by simulations of microwave propagation. A reduction in sample heating at a given microwave power also likely occurs due to reduced dielectric loss. Simulations indicate that the microwave field (and thus the DNP enhancement) is inhomogeneous in the sample, and we deduce that in these experiments between 5 and 10% of the solution actually yields the theoretical maximum signal enhancement of 658. The effect is demonstrated for a variety of particles added to both aqueous and organic biradical solutions.

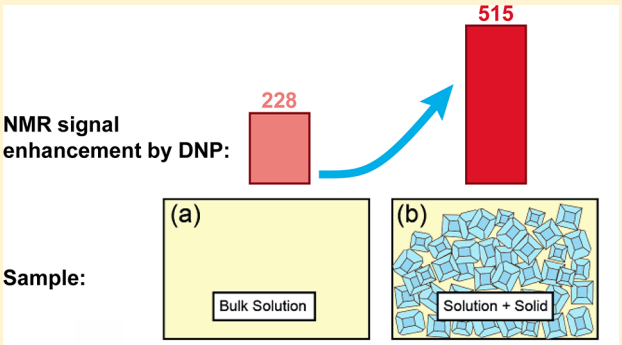

INTRODUCTION

Dynamic nuclear polarization (DNP)[1−3] has recently attracted considerable interest to enhance the sensitivity of both solution and solid-state NMR experiments by several orders of magnitude.[4−9] In a DNP experiment the polarization of unpaired electrons, usually from stable radicals, is transferred to nuclei by applying microwave irradiation to saturate an electron spin transition. This can provide a theoretical maximum NMR signal enhancement of γ_e/γ_n, where γ_e and γ_n are the gyromagnetic ratios of the electron and nucleus in question (γ_e/γ_{1H} = 658, γ_e/γ_{13C} = 2618, γ_e/γ_{15N} = 6494). In both dissolution and magic angle spinning (MAS) DNP experiments, intrinsically diamagnetic samples are usually doped with exogenous radical polarizing agents such as stable trityl or nitroxide radicals.[4,10−12] In dissolution DNP experiments carbon-13 is usually directly polarized, and polarizations above 10% are routinely obtained with low sample temperatures (<5 K). Jannin et al. recently reported polarization of 71% achieved by cross-polarization from protons to carbon-13 at 1.2 K in a magnetic field of 6.7 T.[13] Similarly, with state of the art biradical polarizing agents, proton DNP enhancements (ε_H) of up to 230 and 235 have been reported for organic or aqueous biradical solutions, respectively, with magnetic fields of 5−9.4 T and sample temperatures of ca. 80−105 K.[14−17] These large MAS DNP solid-state NMR signal enhancements have enabled the characterization of a diverse range of chemical systems such as functionalized porous materials,[7,18−21] polymers,[22,23] nanoparticles,[7,21,24,25] pharmaceuticals,[26−28] and several biomolecular systems[29−40] that would have otherwise been inaccessible. Similarly, dissolution DNP has enabled many novel magnetic resonance experiments that hold great promise for improved detection of cancers,[8,9,41,42] better understanding of metabolic pathways,[9,43,44] and applications in chemistry.[21,45] The key to all of these applications is obtaining large DNP enhancements that translate into greatly improved sensitivity for magnetic resonance experiments.

As a result, there is currently great interest in understanding the factors that limit DNP enhancements (e.g., polarizing agents, hardware, MAS rate, temperature, etc.). Here we show

Received: August 27, 2014
Published: October 6, 2014

   dx.doi.org/10.1021/ja5088453 | J. Am. Chem. Soc. 2014, 136, 15711−15718

that over a 2-fold improvement in cross-effect (CE) DNP enhancements can be achieved in MAS DNP experiments of frozen solutions by incorporating solid particles into the samples. At 9.4 T and ∼105 K enhancements up to ε_H = 515 have been obtained, corresponding to 78% of the theoretical maximum. We link this effect to the dielectric properties of the solid material, which give rise to scattering, diffraction, and amplification of the microwave field in the sample, substantiated by simulations of microwave propagation, and to a reduction in sample heating at a given microwave power due to reduced dielectric loss. In passing we also notice that thorough degassing of the sample is crucial to achieve highest enhancements. The effect is demonstrated for a variety of particles added to both aqueous and organic biradical solutions.

EXPERIMENTAL SECTION

All DNP experiments were carried out on a commercial Bruker Avance III 400 MHz NMR spectrometer equipped with a 263 GHz gyrotron microwave source using a 3.2 mm triple resonance MAS probe at sample temperatures around 100 K.[46] In general the microwave power was optimized to obtain the largest DNP enhancements, although the variation in enhancement with microwave power is discussed below for some samples. The magnet sweep coil was used to set the main magnetic field so that microwave irradiation occurred at the maximum positive enhancement for a sample containing TOTAPOL. Proton DNP enhancements (ε_H) were directly measured using a spin echo pulse sequence with a single rotor cycle echo delay to remove probe background signals. The ^{1}H−^{13}C cross-polarization (CP) DNP enhancements ($\varepsilon_{C\,CP}$) were measured with a standard ramped CP pulse sequence. Since the ^{1}H−^{13}C CP signal is observed, $\varepsilon_{C\,CP}$ corresponds to the proton enhancements of the frozen solution. In all cases measured values of ε_H and $\varepsilon_{C\,CP}$ differed by less than 5%. In most cases ε was measured by comparing the intensity of the spectrum acquired with microwave irradiation to that acquired without. In some cases integrated intensities were compared to determine $\varepsilon_{C\,CP}$ in order to account for line narrowing arising from microwave induced sample heating. More details on the NMR parameters and spectra used for DNP enhancement measurements are in the Supporting Information.

The mixed solution-solid material samples were prepared by placing a weighed amount of dry material into a sapphire MAS rotor. The materials were chosen based on their dielectric constants and loss tangents to cover various possible mutual relations of these two parameters.[47] The biradical solution was then added to the loosely packed crystalline material with a micropipette and the liquid was distributed throughout the rotor by gently stirring with a syringe or copper wire. All samples were weighed to determine the precise composition of the sample. Samples were topped with a PTFE insert or silicone plug to prevent solution leakage from the rotors. All samples were weighed before and after performing the experiments to confirm that no loss of solution occurred. Exact compositions of the samples are given in the Supporting Information. Since 95/5 (v/v) solutions of dichloromethane and methanol have been reported to be a good glass forming solutions,[50] a small amount of fully deuterated methanol-d_4 (ca. 4−6% by volume) was added to improve glass formation in the TCE solutions.

Samples were partially degassed inside the low temperature DNP probe by leaving them under a constant nitrogen flow from the sample eject gas for approximately 5 min at room temperature prior to first insertion into the probe at ∼100 K. The samples were then inserted and an array of DNP solid-state NMR experiments was performed (^{1}H and ^{13}C CP DNP enhancement measurements, T_1 measurements, etc.). Samples were then ejected to the base of the probe and subjected to another 5 min of eject gas flow. In this way insert−eject (i.e., freeze−thaw) cycling for each sample was then performed until a constant DNP enhancement signal build-up rate (T_{DNP}) was measured for the ^{1}H nuclei of the solution, as discussed below. Sample temperatures were determined by measuring ^{79}Br longitudinal relaxation times of crystalline KBr.[48] (see Supporting Information for further details)

Finite integral simulations were carried out using the commercial software package CST Microwave Studio 2013 (CST AG, Darmstadt, Germany). The systematic sweep of filling factors and epsilon values was performed on a cylindrical geometry with dimensions similar to that of a 3.2 mm sapphire rotor. Dielectric material properties according to published literature data[47] were assigned to all materials. The mesh resolution in the whole structure was automatically generated, resulting in variable mesh density throughout the model due to different materials with varying dielectric constant. Within the sample region, it was manually refined such that the solution/solid structure within the sample was well resolved, resulting in mesh cells of approximately (50 μm)^3. In all cases, the microwave irradiation was modeled by using a Gaussian Beam at 263 GHz as field source. The transient time domain solver was used for calculating the electromagnetic fields.

RESULTS

The Effect of Incorporating Solid Particles. Figure 1 shows a comparison of proton DNP enhancement factors (ε_H or $\varepsilon_{C\,CP}$) obtained for the NMR resonances of the frozen solution. In one experiment the sample was a bulk solution of a given biradical and in the other experiment the sample comprised the same solution filled into a rotor containing solid particles of crystalline potassium bromide (KBr), sapphire (α-Al_2O_3), calcium fluoride (CaF_2), and sodium chloride (NaCl). In all cases the observed enhancement is significantly higher when the solid particles are present in the sample, reaching values between 450 and 515 (or more than 2.5 times

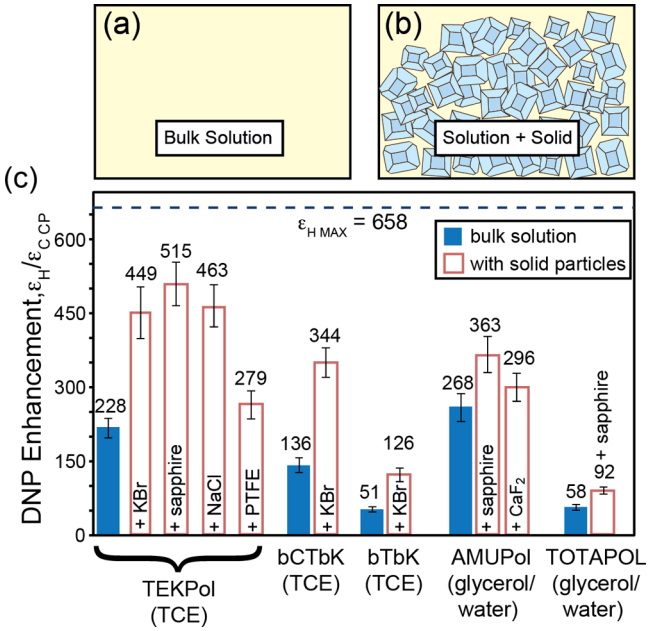

Figure 1. The two types of samples used here are schematically represented in (a) and (b). (c) Comparison of the carbon-13 CP MAS DNP enhancements ($\varepsilon_{C\,CP}$) obtained at 9.4 T with sample temperatures of 100 K observed on the resonances of the frozen solution for various biradicals in bulk solutions (blue, filled) and when the solution is filled into rotors containing solid particles (red columns, open) of either KBr, sapphire, NaCl, polytetrafluoroethylene (PTFE) or CaF_2. For sapphire and PTFE the ^{1}H enhancement was measured directly. Further details are given in the Experimental Section. The dashed line indicates the theoretical maximum achievable proton enhancement of 658.

dx.doi.org/10.1021/ja5088453 | J. Am. Chem. Soc. 2014, 136, 15711−15718

the bulk solution value) for the biradical TEKPol[14] dissolved in 1,1,2,2-tetrachloroethane (TCE)/methanol-d_4 94/6 (v/v) solution. The effect does not change significantly from one radical to another, as the relative gain in enhancement is roughly the same for TEKPol, bCTbK, and bTbK solutions. Furthermore, the effect is not limited to nonpolar organic solvents such as TCE but is also observed in water-based systems, as exemplified by the TOTAPOL[49] or AMUPol biradicals[16] dissolved in 60/30/10 glycerol-d_8/D_2O/H_2O mixed with ground sapphire (having particle sizes of around 300−500 μm), however the relative gain in enhancement is reduced. Notably, when poly(1,1,2,2-tetrafluoroethylene) (PTFE) particles are mixed with the TEKPOL/TCE solution, then the increase in enhancement is more modest, and is discussed below. Figure S1 (Supporting Information) compares the enhancements obtained for TEKPol/TCE solutions mixed with KBr particles of different sizes (with solid volume fractions of ca. 65% in all cases). As shown in Figures S1−S5, larger KBr particle sizes centered around 0.4 mm in diameter provide the largest enhancements, although the effect is not strongly dependent upon particle size, with finely ground KBr giving an enhancement of 360. In all these cases, the solutions have been degassed prior to the measurement, as discussed in the following section.

The Effect of Degassing. It is important to note that the enhancement reported for TCE solutions is the highest value obtained for each sample. Specifically, we previously observed that repeated insertion and ejection of the rotor containing bulk TEKPol/TCE solutions led to improved MAS DNP enhancements.[14] One result of these cycles is to obtain better glass formation in pure TCE, since the quality of the glass formed by pure TCE is variable. It is well-known that chloroform:methanol 95:5 solutions are reliable glass formers,[50] and we observe here that glass formation in TCE can be improved by addition of ∼5% methanol-d_4 by volume, and these conditions are used throughout. Additionally, Figure 2a shows that repeatedly inserting the sample into the cold MAS stator and ejecting it to the base of the probe (i.e., freeze−thaw cycling) leads to the progressive increase in the proton T_1 from 2.7 to 3.5 s for 16 mM TEKPol TCE solution mixed with KBr. The same trend is observed for both bulk and particle containing solutions. This increase is accompanied by gradual growth of the enhancement factor from around 250 to 450 shown in Figure 2b for TEKPol in TCE with KBr. We ascribe this result to progressive removal of dissolved oxygen from the solution in the pure nitrogen atmosphere inside the probe. Since O_2 is paramagnetic its removal increases both electron and nuclear relaxation times, which positively affects DNP efficiency.[51,52] A detailed summary of insert/eject cycling for bulk solution and mixed solutions is given in the Supporting Information (Figures S7−S8 and Tables S2−S5).

Rosay previously reported that fully degassed aqueous 60 mM 4-amino-TEMPO solutions had a proton T_1 of 8.2 s and provided ε_H of 44, while solutions prepared under air had a T_1 of 4.5 s and gave ε_H of 25.[51] Under standard pressure, the concentration of dissolved O_2 in aqueous solutions is approximately 0.5 mM at 298 K. Organic solvents such as TCE usually have much lower surface tension, and under standard conditions the concentration of O_2 should be substantially higher (∼6.5 mM for CCl_4 at 298 K or ∼39 mM for $CHCl_3$ at 298 K).[53] Therefore, the impact of dissolved O_2 on DNP enhancements could be larger for organic solvents. When determining maximum values of ε for organic solvents

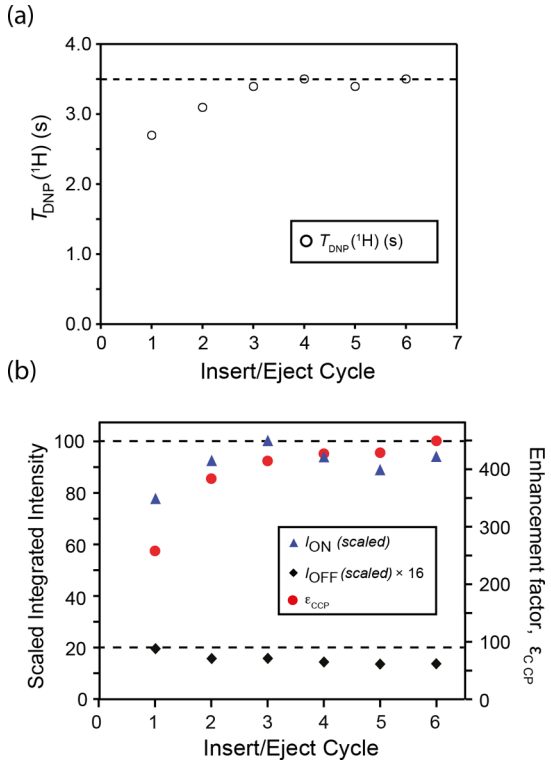

Figure 2. In situ removal of dissolved oxygen from a 16 mM solution of TEKPol in TCE:methanol-d_4 (94:6 v/v) mixed with KBr crystals in a 3.2 mm sapphire rotor. (a) DNP enhanced proton longitudinal polarization build-up times (T_{DNP}) measured with a ^{13}C detected CP saturation recovery pulse sequence as a function of insert−eject cycle. (b) The scaled integrated intensities of the ^{13}C CPMAS spectra acquired with and without microwave irradiation and DNP enhancements for each insert−eject cycle. The intensities are corrected by a scaling factor (s) to remove the effect of relaxation on the absolute intensities calculated for each point as $s = [1 - \exp(\tau_{pd}/T_{DNP,b})]/[1 - \exp(\tau_{pd}/T_{DNP,a})]$ where τ_{pd} is the polarization delay (4 s in all cases), $T_{DNP,b}$ is the T_{DNP} measured for the final cycle number b (here $T_{1,6}$ = 3.5 s), and $T_{DNP,a}$ is the T_1 measured for a given cycle a.

(such as TCE) prepared under ambient conditions it is therefore important to perform insert−eject cycles (or some other degassing procedure) and to measure proton T_1's to assess the amount of dissolved oxygen present in solution. The T_{DNP} dependence and the enhancement factors in Figure 2 converge as the sample is cycled, indicating nearly complete removal of the O_2 dissolved in the solution. We also note that the gain in enhancement due to degassing does not necessarily lead to better overall sensitivity, since the intensity of the microwave off spectrum in Figure 2b continuously decreases, and the T_{DNP} (and thus the polarization delay required for optimal sensitivity) becomes longer. The decrease in the microwave off signal observed for both bulk and particle containing solutions is possibly due to an increase in the so-called "Thurber effect" as longer electron T_{1e} are associated with an increase in MAS induced cross effect nuclear depolarization.[54] Finally, we note that the in situ degassing procedure had no effect on the glycerol/water solutions. This could be because it is more difficult to remove the dissolved oxygen from the aqueous mixture that has higher surface tension, or that the concentration of oxygen is lower and does not affect the DNP enhancements substantially.

dx.doi.org/10.1021/ja5088453 | J. Am. Chem. Soc. 2014, 136, 15711−15718

DISCUSSION

It is unlikely that the solid particles and the solution are interacting in some way that intrinsically changes the DNP effects in these samples. Rather, this effect is most probably due to the fact that the observed proton enhancement for the whole sample is not a microscopic property.[55] The enhancement varies as a function of position in the sample and can be described as an integral over the sample region, R:

$$\bar{\varepsilon} = \frac{1}{V} \iiint_R \varepsilon(x, y, z)\, dV \quad (1)$$

where V is the total volume of the region.

In this light, there are several mechanisms that might explain the effects observed here. The first would be that the solids used here are less lossy than the solutions of TCE or H_2O, and therefore that we obtain better overall microwave penetration into the samples when they are mixed with the particles. The second is that the microstructure created by the solid particles might either concentrate the microwaves in the regions containing the frozen solutions or lead to a better distribution of the microwaves over the sample due to scattering or diffraction phenomena (the particles used here are distributed around 200−400 μm, and the wavelength is ∼1.1 mm). A third, trivial, explanation could be that bulk sample heating is reduced in the samples containing the particles due to less microwave absorption.

Figure 3 compares the measured enhancements and sample heating for bulk solutions of TEKPol in TCE with those for the same solution mixed with crystalline KBr, as a function of the applied microwave power. Figure 3a shows that the sample temperature are quite similar for bulk solution and solution mixed with KBr (temperature increase of ca. 14 and 12 K at the highest microwave power, respectively). This confirms that the increase in enhancement does not arise from reduced sample temperatures that would lead to higher CE DNP performance. Figure 3a also shows that, in contrast to the solutions, a sample of pure ground KBr heats much less significantly over this range of powers (ca. 4 K at maximum power). This suggests that the samples including KBr are indeed less lossy, suggesting that both of the first two mechanisms discussed above may play a role.

Figure 3b shows the enhancements obtained for both samples as a function of the applied microwave power. In both samples the enhancement continuously increases with the applied microwave power although at elevated powers above 7 W the increase in enhancement is reduced. At elevated microwave powers the ^{13}C CPMAS spectra begin to narrow due to a temperature increase (Figure S6). Therefore, integrated intensities were used to measure the enhancements in order to better account for differences in line widths. Hu et al. have previously shown that a plot of $1/\varepsilon$ versus the inverse of the microwave power $(1/P)$ yields a straight line that can be fit to the equation:

$$\frac{1}{\varepsilon} = \frac{1}{\varepsilon_\infty}\left(1 + \frac{1}{aP}\right) \quad (2)$$

where ε_∞ is the DNP enhancement at infinite microwave power and a is the saturation parameter.[56,57] The saturation parameter depends upon the electron relaxation times (T_{1e} and T_{2e}) and the microwave transmission efficiency of the sample. The plot in Figure 3c shows that for both bulk TEKPol/TCE solution and the solution mixed with KBr, ε_∞ of 680 and 690 are obtained, respectively. This suggests that TEKPol can potentially provide the theoretical maximum proton DNP enhancement of 658. However, a, which can be measured from the data in Figure 3c, was found to be nearly three times higher for the solution mixed with KBr. Since the electron relaxation times will be the same in both samples, this is consistent with substantially improved microwave transmission in the mixed sample.

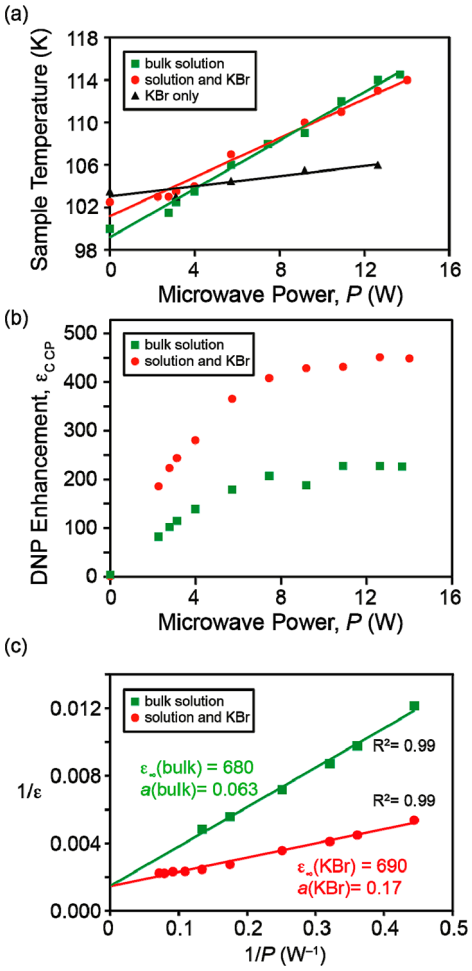

Figure 3. (a) The variation in sample temperature as a function of the applied microwave power for bulk 16 mM TEKPol in TCE:methanol-d_4 (94:6 v/v) solution, the same solution mixed with KBr, and pure KBr (no solution added). The solid lines are visual guides. (b) Proton DNP enhancement as a function of applied microwave power for bulk solution and solution mixed with KBr. (c) Inverse of the DNP enhancement $(1/\varepsilon)$ as a function of the inverse of microwave power $(1/P)$ for bulk solution and a solution mixed with KBr. Linear fits are shown as solid lines. The DNP enhancement at infinite microwave power (ε_∞) was obtained from the intercept and the saturation factor (a) was calculated from the intercept and slope. Note that if the high microwave power points are included in the fit for the bulk solution, there is deviation from the straight line behavior, and a lower ε_∞ (of ca. 400) is obtained. However, since there is substantial sample heating at high microwave powers, the four highest power points for the bulk solution were excluded from the plot. Sample temperatures were measured from the spin−lattice relaxation rate of ^{79}Br (in case of bulk solutions a small amount of KBr was placed at the bottom of the rotor).[48]

In order to better understand the factors that yield high enhancements for crystal/solution mixtures finite element simulations of microwave propagation were performed. Figure

dx.doi.org/10.1021/ja5088453 | J. Am. Chem. Soc. 2014, 136, 15711−15718

4a shows the models of static samples corresponding to a sapphire rotor filled with varying ratios of solution (yellow regions) and solid particles (green regions). The models were generated by random filling with ellipsoids of different sizes distributed between 0.15 and 0.5 mm. Finite element simulations of this kind have previously been used by Nanni et al. to optimize the rotor and coil geometries in MAS DNP.[55] Notably, their simulations predicted that when a homogeneous solution in a sapphire rotor is irradiated through a solenoidal coil the microwave field is inhomogeneous over the sample volume. The simulation in Figure 4b reproduces this finding. In our simulations the real component of the dielectric constant of the solution was set to 2.5 for the solvent (TCE) region because similar values are reported for many organic materials,[47] while the loss tangent (tan δ) was 0.009 (based upon the value measured by Nanni et al. for water-glycerol, and scaled by the microwave frequency).

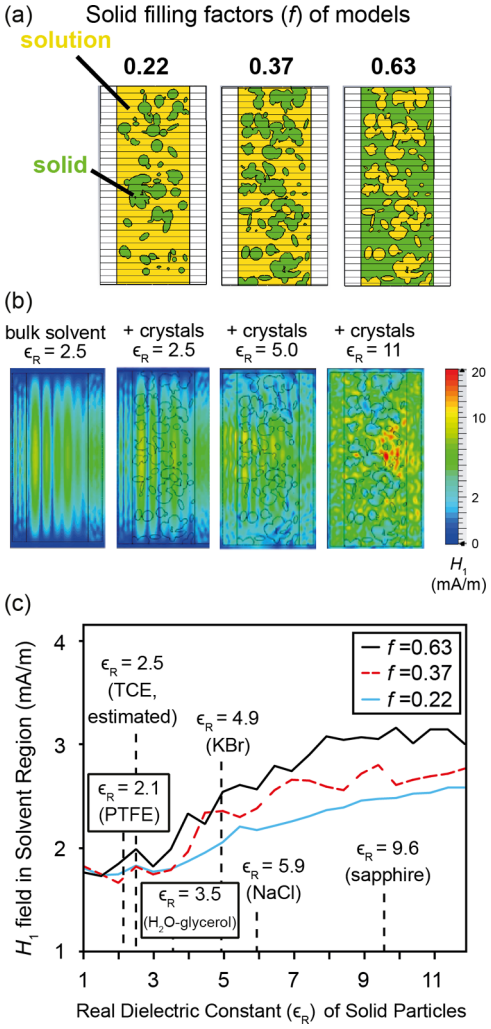

Figure 4. Finite element simulations of microwave propagation in (a) a model of a sapphire rotor filled with different filling factors of dielectric particles ($f = V_{solid}/V_{total}$) and frozen solution (green and yellow areas, respectively). (b–e) Cross sections showing the calculated transverse magnetic component of the microwave field (H_1) for (b) bulk solution and (c–e) rotors filled with 63% solid particles and 37% solution. For (c–e) the real component of the dielectric constant ϵ_r of the solid particles is indicated. (f) The average H_1 field predicted for the solution region, as a function of the real component of the dielectric constant of the solid particles and different particle filling factors. Known real components of the dielectric constant are indicated for several materials. Details of the finite integral simulations are given in the main text and Experimental Section.

Figure 4b show the field distributions for a solution with 63% of space occupied by solid particles with varying real components of the dielectric constant (ϵ_r). Note that both the DNP enhancement and the real component of the dielectric constant are designated by the symbol epsilon. Here the former are indicated as ε and the latter as ϵ_r. The loss tangent was set to 0.001 for the particles in all cases (a factor of nine lower than that of the solution region). In Figure 4c the real component of the dielectric constant of the solid particles matches that of the solution. In this case only a slight increase in average microwave field in the sample is predicted (Figure 4f), presumably due to reduced lossiness associated with the solid regions of the sample. This rationalizes the small increase in DNP enhancement observed for a solution mixed with PTFE particles (Figure 1). PTFE has a dielectric constant (2.0) that is probably similar to that of the TCE solution and is well-known to have a low dielectric loss.[47]

Figure 4d,e shows the same simulation but for solids with a real component of the dielectric constant of 5, similar to that reported for KBr ($\epsilon_r = 4.9$), and of 11.0. We clearly observe that when the dielectric constant of the solid and the solution are mismatched, the microwave field distribution is substantially modified, and the average microwave field in the solution region of the sample substantially increases (Figure 4f). Figure 4b–e illustrates that the simulations predict that there are very intense hot spots inside the particles.

In Figure 4f the average microwave field in the solution region is plotted as a function of ϵ_r for several different filling factors. It can be concluded that by using a material with an increasingly mismatched real dielectric constant compared to that of the frozen solution (and with a lower loss tangent), it is in principle, possible to increase the average microwave field over the whole sample volume by a factor of nearly 2. Under our experimental conditions we estimate that the filling factors are around 0.65, where we predict the average microwave field to be increased by a factor ~1.5 for KBr ($\epsilon_r = 4.9$), and by a factor of ~1.8 for sapphire ($\epsilon_r = 9.6$). However, as previously discussed by Nanni et al., to properly calculate DNP enhancements the distribution of microwave field in the sample should be considered, not just the average values.[55]

Figure 5 shows histograms of the relative probability of a given transverse magnetic component (H_1) of the microwave field in the sample as obtained from the finite element simulations above. The histograms are plotted both for the bulk solution model of Figure 4b and for models of solvent mixed with solid particles with several different ϵ_r values for the solid particles as in Figure 4c–e. The H_1 values from simulations can then be converted to electron nutation frequencies (ν_1):

$$\nu_1 = \gamma_e \mu_0 H_1 (cP_{in}/P_{sim})^{1/2} \quad (3)$$

where γ_e is the gyromagnetic ratio of the electron (28.016 GHz/T), μ_0 is the permittivity of free space ($4\pi \times 10^{-7}$ N·A^{-2}), H_1 is the calculated magnetic field in mA/m, c is a dimensionless constant that corresponds to the fraction of power delivered to the sample, P_{sim} is the finite element simulation input power (8.34 nW in all cases) and P_{in} is the experimentally measured input power at the output of the waveguide. The top horizontal axis of Figure 5 shows the

dx.doi.org/10.1021/ja5088453 | J. Am. Chem. Soc. 2014, 136, 15711–15718

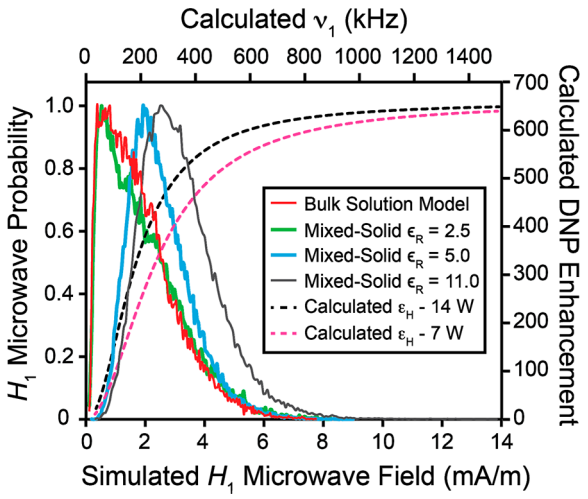

Figure 5. (a) The distribution of calculated H_1 field values for the bulk solution model and mixed solid-solution models from Figure 4b–e. The calculated H_1 values were converted to electron nutation frequencies with eq 3 assuming 14 W of input power (ν_1, top axis). The H_1 values were then converted to DNP enhancements with eq 3 and 4 for both 7 and 14 W of input power (right axis, dashed lines).

corresponding ν_1 values with P_{in} = 14 W and c = 0.27. The determination of c, which is here treated as a simple adjustable scaling factor between the experiment and the simulation to account for attenuation in the probe, is discussed below.

The simulated histogram of microwave fields shows that in the bulk solvent model ν_1 is generally low in most of the sample with a mode of only 41 kHz. However, in the mixed samples the histograms clearly illustrate a large shift in the distributions of ν_1 to higher frequencies. For solids with ϵ_r of 5.0 and 11.0 the mode of the ν_1 distribution shifts to 208 kHz and 271 kHz, respectively. Also, note that there is a large tail in the mixed samples with low populations of high ν_1 out to as high as 1.4 MHz for ϵ_r = 11.0.

The calculated ν_1 values can be converted to DNP enhancements with the following equation:[55]

$$\varepsilon = \varepsilon_\infty \left(\frac{\alpha(\nu_1)^2}{1 + \alpha(\nu_1)^2} \right) \quad (4)$$

Here ε_∞ is the DNP enhancement at infinite microwave power, α is the saturation factor ($\alpha = T_{1e}T_{2e}/2$), where T_{1e} and T_{2e} are the longitudinal and transverse relaxation times of the electron, respectively.[55] Here we take $T_{1e}T_{2e}$ = 60 μs^2 based upon previous 94 GHz EPR measurements of electron relaxation times in 16 mM TEKPol TCE solutions, which fixes the value of α.[14] Upon the basis of the measured dependence of DNP enhancement on the microwave power (Figure 3), ε_∞ of 658 was used.

The calculated enhancements are shown as the two dashed lines in Figure 5 for 14 and 7 W of input power. By considering the weighting of the H_1 distributions in the two models, the volume averaged DNP enhancement ($\bar{\varepsilon}$) can then be calculated (Table 1). In comparison with the data in Figure 3, if the value of c is set to 0.27 in eq 3, then an $\bar{\varepsilon}$ of 219 is calculated for 7 W of input power in the bulk solution model, which is in good agreement. By comparison, 14 W of input power is then predicted to give an $\bar{\varepsilon}$ of 298 for the bulk solution model, which is larger than the measured value of 226. However, we note that in the bulk solution there is substantial sample heating at higher powers, and measured enhancements do not increase very much at higher powers.

Table 1. Summary of Finite Element Simulations

model	calculated $\bar{\varepsilon}$, P_{in} = 7 W	calculated $\bar{\varepsilon}$, P_{in} = 14 W	comparable experimental ε
bulk solution (4b)	219	298	228
mixed with ϵ_r 2.5 solid (4c)	232	309	289 (PTFE)
mixed with ϵ_r 5.0 solid (4d)	321	418	449 (KBr)
mixed with ϵ_r 11.0 solid (4d)	389	478	515 (sapphire)

Better agreement with experiment is seen for the model of the mixed sample and a solid with ϵ_r of 2.5 (and a reduced loss tangent, see above). In this case an $\bar{\varepsilon}$ of 289 is predicted, in good agreement with the experimental value obtained for solution mixed with PTFE particles (Table 1). For 14 W of input power, the calculated H_1 distribution for the mixed solid-solution model, ϵ_r = 5.0 and the same c value, $\bar{\varepsilon}$ of 418 is predicted, again in reasonable agreement with the measured ε_{CCP} values of 449 for TCE solution mixed with KBr. Reasonably good agreement is also seen with the experimental values for sapphire crystals and the highest dielectric constant of 11.0 included in the model (Table 1, $\bar{\varepsilon}$ = 478 and ε_H = 515).

Interestingly, with 14 W of input power the simulations predict that in the mixed model with ϵ_r = 11 for the solid particles, 28% of the sample actually yields DNP enhancements above 550. Further, when the input power in the simulation is increased to 19.7 W for the mixed solution-solid with dielectric 11, then the predicted value of $\bar{\varepsilon}$ is increased to agree with the measured value for sapphire of 515 (Figure 1) (note this could also be achieved by changing the value of c). Under these conditions we find that with the distribution having the shape of that in Figure 5 (ϵ_r = 11), *14% of the sample now yields enhancements above 600, essentially reaching the theoretical maximum.*

In summary, the simulations predict a large increase in the microwave field inside the mixed dielectric sample that can explain the increased DNP enhancements.

Of course, here we have focused on an explanation in terms of the interaction of scattering and diffusion of the microwaves. Other explanations that we have not yet envisaged may be possible, and further studies will be required to firmly establish the exact nature of the effect.

CONCLUSIONS

We have demonstrated that by mixing insoluble solid particles of relatively high dielectric constant with biradical solutions, MAS DNP enhancements can be increased by a factor of over two. We also note that to obtain these high enhancements it is crucial to deoxygenate the samples. Removal of oxygen can conveniently be performed in situ by repeatedly inserting and ejecting the sample and subjecting it to several minutes of room temperature nitrogen gas flow at the base of the probe. Simulations of microwave propagation suggest that the increased enhancements arise because high dielectric materials create microstructures that diffract or more generally scatter the incident beam in a manner that leads to a significant redistribution of the field, and which in turn leads to a large increase in the average microwave field experienced by the solution. Experimentally, particles with sizes on the order of 100 to 500 μm seem to provide the largest gains in DNP

dx.doi.org/10.1021/ja5088453 | J. Am. Chem. Soc. 2014, 136, 15711–15718

enhancement, although gains in ε can still be obtained with smaller particles, such as finely ground microcrystalline powders (e.g., $\varepsilon_{C\,CP}$ = 360 ± 36 for TEKPol/TCE incorporating finely ground KBr), and the effect is present in DNP enhanced experiments on, for example, finely ground organic powders (Figure S12). In the case of finely ground organic solids that are themselves the target to be polarized, the gain in enhancements translates to improved sensitivity.

A particularly important consequence of this work is that the TEKPol/TCE polarizing system is probably capable of providing the theoretical maximum enhancements at 9.4 T and 100 K. We deduce this since there is certainly still a distribution of the microwave field in the samples containing particles with high dielectrics (Figure 5), so that to observe an average epsilon of 515 in the case of sapphire, the DNP enhancement in parts of the sample must be above 600. We conclude that with improved coupling of the microwaves to the sample, current state-of-the-art DNP polarizing agents could provide ε_H near to the theoretical limit of 658.

Finally, we note that the addition of the solid particles to the rotor does not improve absolute sensitivity, since the gain in ε_H is here offset by a reduction in active sample volume. Therefore, this approach would only improve overall sensitivity for samples that are mass limited. However, in the light of the findings here, it should be possible to engineer dielectric microstructures within the rotor to increase the microwave field and obtain higher enhancements without occupying such a significant volume. This approach may also be applicable to other DNP techniques, such as dissolution DNP. We are currently investigating such possibilities.

■ ASSOCIATED CONTENT

Supporting Information

Additional experimental details, sample compositions, grain size distributions of solid materials, measurements of DNP enhancements. This material is available free of charge via the Internet at http://pubs.acs.org.

■ AUTHOR INFORMATION

Corresponding Author

lyndon.emsley@ens-lyon.fr

Notes

The authors declare no competing financial interest.

■ ACKNOWLEDGMENTS

We thank Claire Sauvée and Dr. Gilles Casano (Universite Aix-Marseille) for synthesizing the biradicals used here. We thank Bruker France and Drs. Alain Belguise and Fabien Aussenac for providing initial access to the DNP spectrometer. This work was supported by ERC Advanced Grant No. 320860.

■ REFERENCES

(1) Carver, T. R.; Slichter, C. P. *Phys. Rev.* **1953**, *92*, 212−213.

(2) Abragam, A.; Goldman, M. *Nuclear Magnetism: Order and Disorder (Monographs on Physics)*; Oxford University Press: Oxford, U.K., 1982.

(3) Goldman, M. *Spin Temperature and Nuclear Magnetic Resonance in Solids (Monographs on Physics)*; Oxford University Press: Oxford, U.K., 1970.

(4) Ardenkjaer-Larsen, J. H.; Fridlund, B.; Gram, A.; Hansson, G.; Hansson, L.; Lerche, M. H.; Servin, R.; Thaning, M.; Golman, K. *Proc. Natl. Acad. Sci. U. S. A.* **2003**, *100*, 10158−10163.

(5) Becerra, L. R.; Gerfen, G. J.; Temkin, R. J.; Singel, D. J.; Griffin, R. G. *Phys. Rev. Lett.* **1993**, *71*, 3561−3564.

(6) Hall, D. A.; Maus, D. C.; Gerfen, G. J.; Inati, S. J.; Becerra, L. R.; Dahlquist, F. W.; Griffin, R. G. *Science* **1997**, *276*, 930−932.

(7) Lesage, A.; Lelli, M.; Gajan, D.; Caporini, M. A.; Vitzthum, V.; Miéville, P.; Alauzun, J.; Roussey, A.; Thieuleux, C.; Mehdi, A.; Bodenhausen, G.; Copéret, C.; Emsley, L. *J. Am. Chem. Soc.* **2010**, *132*, 15459−15461.

(8) Albers, M. J.; Bok, R.; Chen, A. P.; Cunningham, C. H.; Zierhut, M. L.; Zhang, V. Y.; Kohler, S. J.; Tropp, J.; Hurd, R. E.; Yen, Y.-F.; Nelson, S. J.; Vigneron, D. B.; Kurhanewicz, J. *Cancer Res.* **2008**, *68*, 8607−8615.

(9) Gallagher, F. A.; Kettunen, M. I.; Day, S. E.; Hu, D. E.; Ardenkjaer-Larsen, J. H.; in't Zandt, R.; Jensen, P. R.; Karlsson, M.; Golman, K.; Lerche, M. H.; Brindle, K. M. *Nature* **2008**, *453*, 940−U973.

(10) Hwang, C. F.; Hill, D. A. *Phys. Rev. Lett.* **1967**, *18*, 110−112.

(11) Afeworki, M.; McKay, R. A.; Schaefer, J. *Macromolecules* **1992**, *25*, 4084−4091.

(12) Maly, T.; Debelouchina, G. T.; Bajaj, V. S.; Hu, K. N.; Joo, C. G.; Mak-Jurkauskas, M. L.; Sirigiri, J. R.; van der Wel, P. C. A.; Herzfeld, J.; Temkin, R. J.; Griffin, R. G. *J. Chem. Phys.* **2008**, *128*, 052211.

(13) Jannin, S.; Bornet, A.; Melzi, R.; Bodenhausen, G. *Chem. Phys. Lett.* **2012**, *549*, 99−102.

(14) Zagdoun, A.; Casano, G.; Ouari, O.; Schwarzwälder, M.; Rossini, A. J.; Aussenac, F.; M, Y.; G, J.; Copéret, C.; Lesage, A.; Tordo, P.; Emsley, L. *J. Am. Chem. Soc.* **2013**, *135*, 12790−12797.

(15) Zagdoun, A.; Casano, G.; Ouari, O.; Lapadula, G.; Rossini, A. J.; Lelli, M.; Baffert, M.; Gajan, D.; Veyre, L.; Maas, W. E.; Rosay, M.; Weber, R. T.; Thieuleux, C.; Copéret, C.; Lesage, A.; Tordo, P.; Emsley, L. *J. Am. Chem. Soc.* **2012**, *134*, 2284−2291.

(16) Sauvée, C.; Rosay, M.; Casano, G.; Aussenac, F.; Weber, R. T.; Ouari, O.; Tordo, P. *Angew. Chem., Int. Ed.* **2013**, *52*, 10858−10861.

(17) Kiesewetter, M. K.; Corzilius, B.; Smith, A. A.; Griffin, R. G.; Swager, T. M. *J. Am. Chem. Soc.* **2012**, *134*, 4537−4540.

(18) Lelli, M.; Gajan, D.; Lesage, A.; Caporini, M. A.; Vitzthum, V.; Miéville, P.; Héroguel, F.; Rascon, F.; Roussey, A.; Thieuleux, C.; Boualleg, M.; Veyre, L.; Bodenhausen, G.; Copéret, C.; Emsley, L. *J. Am. Chem. Soc.* **2011**, *133*, 2104−2107.

(19) Lafon, O.; Rosay, M.; Aussenac, F.; Lu, X.; Trébosc, J.; Cristini, O.; Kinowski, C.; Touati, N.; Vezin, H.; Amoureux, J. P. *Angew. Chem., Int. Ed.* **2011**, *50*, 8367−8370.

(20) Grüning, W. R.; Rossini, A. J.; Zagdoun, A.; Gajan, D.; Lesage, A.; Emsley, L.; Copéret, C. *Phys. Chem. Chem. Phys.* **2013**, *15*, 13270−13274.

(21) Lafon, O.; Thankamony, A. S. L.; Kobayashi, T.; Carnevale, D.; Vitzthum, V.; Slowing, I. I.; Kandel, K.; Vezin, H.; Amoureux, J. P.; Bodenhausen, G.; Pruski, M. *J. Phys. Chem. C* **2013**, *117*, 1375−1382.

(22) Blanc, F.; Chong, S. Y.; McDonald, T. O.; Adams, D. J.; Pawsey, S.; Caporini, M. A.; Cooper, A. I. *J. Am. Chem. Soc.* **2013**, *135*, 15290−15293.

(23) Ouari, O.; Phan, T.; Ziarelli, F.; Casano, G.; Aussenac, F.; Thureau, P.; Gigmes, D.; Tordo, P.; Viel, S. *ACS Macro Lett.* **2013**, *2*, 715−719.

(24) Vitzthum, V.; Miéville, P.; Carnevale, D.; Caporini, M. A.; Gajan, D.; Copéret, C.; Lelli, M.; Zagdoun, A.; Rossini, A. J.; Lesage, A.; Emsley, L.; Bodenhausen, G. *Chem. Commun.* **2012**, *48*, 1988−1990.

(25) Akbey, Ü.; Altin, B.; Linden, A.; Özçelik, S.; Gradzielski, M.; Oschkinat, H. *Phys. Chem. Chem. Phys.* **2013**, *15*, 20706−20716.

(26) Rossini, A. J.; Zagdoun, A.; Hegner, F. S.; Schwarzwälder, M.; Gajan, D.; Copéret, C.; Lesage, A.; Emsley, L. *J. Am. Chem. Soc.* **2012**, *134*, 16899−16908.

(27) Ong, T. C.; Mak-Jurkauskas, M. L.; Walish, J. J.; Michaelis, V. K.; Corzilius, B.; Smith, A. A.; Clausen, A. M.; Cheetham, J. C.; Swager, T. M.; Griffin, R. G. *J. Phys. Chem. B* **2013**, *117*, 3040−3046.

(28) Rossini, A. J.; Widdifield, C. M.; Zagdoun, A.; Lelli, M.; Schwarzwälder, M.; Copéret, C.; Lesage, A.; Emsley, L. *J. Am. Chem. Soc.* **2014**, *136*, 2324−2334.
(29) Van der Wel, P. C. A.; Hu, K. N.; Lewandowski, J.; Griffin, R. G. *J. Am. Chem. Soc.* **2006**, *128*, 10840−10846.
(30) Mak-Jurkauskas, M. L.; Bajaj, V. S.; Hornstein, M. K.; Belenky, M.; Griffin, R. G.; Herzfeld, J. *Proc. Natl. Acad. Sci. U. S. A.* **2008**, *105*, 883−888.
(31) Bajaj, V. S.; Mak-Jurkauskas, M. L.; Belenky, M.; Herzfeld, J.; Griffin, R. G. *Proc. Natl. Acad. Sci. U. S. A.* **2009**, *106*, 9244−9249.
(32) Salnikov, E.; Rosay, M.; Pawsey, S.; Ouari, O.; Tordo, P.; Bechinger, B. *J. Am. Chem. Soc.* **2010**, *132*, 5940−5941.
(33) Linden, A. H.; Lange, S.; Franks, W. T.; Akbey, Ü.; Specker, E.; van Rossum, B.-J.; Oschkinat, H. *J. Am. Chem. Soc.* **2011**, *133*, 19266−19269.
(34) Reggie, L.; Lopez, J. J.; Collinson, I.; Glaubitz, C.; Lorch, M. *J. Am. Chem. Soc.* **2011**, *133*, 19084−19086.
(35) Sergeyev, I. V.; Day, L. A.; Goldbourt, A.; McDermott, A. E. *J. Am. Chem. Soc.* **2011**, *133*, 20208−20217.
(36) Cheng, C. Y.; Wang, J. Y.; Kausik, R.; Lee, K. Y. C.; Han, S. *J. Magn. Reson.* **2012**, *215*, 115−119.
(37) Potapov, A.; Yau, W.-M.; Tycko, R. *J. Magn. Reson.* **2013**, *231*, 5−14.
(38) Ravera, E.; Corzilius, B.; Michaelis, V. K.; Rosa, C.; Griffin, R. G.; Luchinat, C.; Bertini, I. *J. Am. Chem. Soc.* **2013**, *135*, 1641−1644.
(39) Takahashi, H.; Ayala, I.; Bardet, M.; De Paëpe, G.; Simorre, J. P.; Hediger, S. *J. Am. Chem. Soc.* **2013**, *135*, 5105−5110.
(40) Wang, T.; Park, Y. B.; Caporini, M. A.; Rosay, M.; Zhong, L. H.; Cosgrove, D. J.; Hong, M. *Proc. Natl. Acad. Sci. U. S. A.* **2013**, *110*, 16444−16449.
(41) Jindal, A. K.; Merritt, M. E.; Suh, E. H.; Malloy, C. R.; Sherry, A. D.; Kovacs, Z. *J. Am. Chem. Soc.* **2010**, *132*, 1784−1785.
(42) Hurd, R. E.; Spielman, D.; Josan, S.; Yen, Y.-F.; Pfefferbaum, A.; Mayer, D. *Magn. Reson. Med.* **2013**, *70*, 936−942.
(43) Harris, T.; Degani, H.; Frydman, L. *NMR Biomed.* **2013**, *26*, 1831−1843.
(44) Shmidt, R.; Laustsen, C.; Kettunen, M. I.; Dumez, J.-N.; Marco-Rius, I.; Brindle, K. M.; Ardenkjaer-Larsen, J. H.; Frydman, L. *J. Magn. Reson.* **2014**, *240*, 8−15.
(45) Koptyug, I. V.; Kovtunov, K. V.; Burt, S. R.; Anwar, M. S.; Hilty, C.; Han, S.-I.; Pines, A.; Sagdeev, R. Z. *J. Am. Chem. Soc.* **2007**, *129*, 5580−5586.
(46) Rosay, M.; Tometich, L.; Pawsey, S.; Bader, R.; Schauwecker, R.; Blank, M.; Borchard, P. M.; Cauffman, S. R.; Felch, K. L.; Weber, R. T.; Temkin, R. J.; Griffin, R. G.; Maas, W. E. *Phys. Chem. Chem. Phys.* **2010**, *12*, 5850−5860.
(47) Lamb, J. W. *Int. J. Infrared Millimeter Waves* **1996**, *17*, 1997−2034.
(48) Thurber, K. R.; Tycko, R. *J. Magn. Reson.* **2009**, *196*, 84−87.
(49) Song, C. S.; Hu, K. N.; Joo, C. G.; Swager, T. M.; Griffin, R. G. *J. Am. Chem. Soc.* **2006**, *128*, 11385−11390.
(50) Eaton, G. R.; Eaton, S. S.; Barr, D. P.; Weber, R. T. *Quantitative EPR*; Springer: Vienna, 2010.
(51) Rosay, M. Ph.D. Thesis; Massachusetts Institute of Technology: Cambridge, MA, 2001.
(52) Zagdoun, A.; Rossini, A. J.; Conley, M. P.; Grüning, W. R.; Schwarzwälder, M.; Lelli, M.; Franks, W. T.; Oschkinat, H.; Copéret, C.; Emsley, L.; Lesage, A. *Angew. Chem., Int. Ed.* **2013**, *52*, 1222−1225.
(53) Battino, R.; Rettich, T. R.; Tominaga, T. *J. Phys. Chem. Ref. Data* **1983**, *12*, 163−177.
(54) Thurber, K. R.; Tycko, R. *J. Chem. Phys.* **2014**, *140*, 184201−184211.
(55) Nanni, E. A.; Barnes, A. B.; Matsuki, Y.; Woskov, P. P.; Corzilius, B.; Griffin, R. G.; Temkin, R. J. *J. Magn. Reson.* **2011**, *210*, 16−23.
(56) Hu, K. N.; Song, C.; Yu, H. H.; Swager, T. M.; Griffin, R. G. *J. Chem. Phys.* **2008**, *128*, 052301−052317.
(57) Matsuki, Y.; Maly, T.; Ouari, O.; Karoui, H.; Le Moigne, F.; Rizzato, E.; Lyubenova, S.; Herzfeld, J.; Prisner, T.; Tordo, P.; Griffin, R. G. *Angew. Chem., Int. Ed.* **2009**, *48*, 4996−5000.